Multiscale Analysis for Higher-order Tensors

Alp Ozdemir, Mark A. Iwen and Selin Aviyente,

arXiv:1704.08578v1 [cs.NA] 27 Apr 2017

***Abstract*—The widespread use of multisensor technology and the emergence of big data sets have created the necessity to develop more versatile tools to represent large and multimodal data such as higher-order tensors. Tensor decomposition based methods have been shown to be flexible in the choice of the constraints and to extract more general latent components in such data compared to matrix-based methods. For these reasons, tensor decompositions have found applications in many different signal processing problems including dimensionality reduction, signal separation, linear regression, feature extraction, and classification. However, most of the existing tensor decomposition methods are founded on the principle of finding a low-rank approximation in a linear subspace structure, where the definition of the rank may change depending on the particular decomposition. Since most data are not necessarily low-rank in a linear subspace, this often results in high approximation errors or low compression rates. In this paper, we introduce a new adaptive, multi-scale tensor decomposition method for higher order data inspired by hybrid linear modeling and subspace clustering techniques. In particular, we develop a multi-scale higher-order singular value decomposition (MS-HoSVD) approach where a given tensor is first permuted and then partitioned into several sub-tensors each of which can be represented as a low-rank tensor increasing the efficiency of the representation. The proposed approach is evaluated for two different signal processing applications: dimensionality reduction and classification.**

***Index Terms*—higher-order singular value decomposition, tensor decomposition, multi-scale decomposition, data reduction, big data applications.**

I. Introduction

Data in the form of multidimensional arrays, also referred to as tensors, arise in a variety of applications including chemometrics, hyperspectral imaging, high resolution videos, neuroimaging (EEG, fMRI), biometrics and social network analysis [1]–[3]. These applications produce massive amounts of data collected in various forms including large-scale graphs or networks with both multiple aspects and high dimensionality. Tensors, which are multi-dimensional generalizations of matrices, provide a useful representation for such data. Once higher-order tensors have been used to store the inherently multidimensional data, the application will dictate what type of manipulation or postprocessing of the data is required. A crucial step in many applications involving higher-orders tensors is multiway compression of the data to ensure that the compressed representation of the tensor retains certain characteristics. Early multiway data analysis approaches reformatted the tensor data as a matrix and resorted to methods developed for classical two-way analysis. However, one cannot discover hidden components within multiway data using conventional matrix decomposition methods. To this end, many different types of tensor decomposition methods have been proposed in the literature [4]–[8].

In contrast to the matrix case, where compression is often accomplished via low-rank representations such as singular value decomposition (SVD), the notion of rank for higher order tensors is not uniquely defined. CANDECOMP/PARAFAC (CP) decomposition and Tucker decomposition are two of the most widely used tensor decomposition methods [9], [10]. Both of these methods can be seen as higher order generalizations of the matrix SVD and principal component analysis (PCA). For CP, the goal is to approximate the given tensor as a weighted sum of Rank-1 tensors, where Rank-1 tensor refers to the outer product of n vectors with n being the order of the tensor. The motivation behind CP is to obtain a low-rank representation, where the rank R is defined as the smallest value of R for which the sum holds exactly, such that component matrices are determined uniquely up to a permutation and scaling of columns provided that the Kruskal condition is met [11]. Similar to CP, Tucker decomposition is an extension of bilinear factor analysis to higher-order datasets. Tucker decomposition treats a tensor as a multilinear transformation of a typically dense but small core tensor by the factor matrices. Compared to CP, a Tucker model is more flexible due to the core array which allows for interactive bases. Unlike CP decomposition, Tucker decomposition is in general non-unique. To obtain meaningful and unique representation by the Tucker decomposition, orthogonality, sparsity and non-negativity constraints are often imposed on the factors yielding Non-Negative Tensor Factorization (NTF) and Sparse Non-Negative Tucker Decomposition [12]–[14]. Tucker decomposition with orthogonality constraints on the factors, is known as Higher-Order Singular Value Decomposition (HoSVD) or Multilinear SVD [10]. HoSVD can simply be computed by flattening the tensor in each mode and calculating the n-mode singular vectors corresponding to that mode. Tucker model also introduces the notion of a new rank, Tucker rank or n-rank, which refers to the n-tuple of ranks of each of the matrices obtained by flattening the tensor in each mode. An alternative approach to extending the matrix SVD to tensors is the tensor-SVD (t-SVD) which treats multimidensional arrays as linear operators instead of multilinear operators [15], [16]. In this framework, a 3-D tensor is viewed as a matrix of tubes and a tensor is written as a product of 3 third-order tensors similar to the matrix SVD, where the product is given by the circular convolution. This approach has the advantage of transforming the tensor decomposition problem to a simple SVD in the Fourier domain.

A. Ozdemir (ozdemira@egr.msu.edu) and S. Aviyente (aviyente@egr.msu) are with the Electrical and Computer Engineering, Michigan State University, East Lansing, MI, 48824, USA.

Mark A. Iwen (markiwen@math.msu.edu) is with the Department of Mathematics, and the Department of Computational Mathematics, Science, and Engineering (CMSE), Michigan State University, East Lansing, MI, 48824, USA.

This work was in part supported by NSF DMS-1416752 and NSF CCF-1615489.

With the emergence of multidimensional big data, classical tensor representation and decomposition methods have become inadequate since the size of these tensors exceeds available working memory and the processing time is very long. In order to address the problem of large-scale tensor decomposition, several block-wise tensor decomposition methods have been proposed [6]. The basic idea is to partition a big data tensor into smaller blocks and perform tensor related operations block-wise using suitable tensor format. Preliminary approaches relied on a hierarchical tree structure and reduced the storage of d-dimensional arrays to the storage of auxiliary three-dimensional ones such as the tensor-train decomposition (TT-decomposition), also known as the matrix product state (MPS) decomposition, [5] and Hierarchical Tucker Decomposition (HT) [17]. In particular, in the area of large volumetric data visualization, tensor based multiresolution hierarchical methods such as TAMRESH have attracted attention [18]. However, all of these methods are interested in fitting a low-rank model to data which lies near a *linear* subspace, thus being limited to learning linear structure and cannot capture existing nonlinearities.

Recently, to better deal with the curse of dimensionality, both linear and nonlinear subspace learning methods have been extended for higher order data reduction. In early work in the area, Vasilescu and Terzopoulos [19] extended the eigenface concept to the tensorface by using higher order SVD and taking different modes such as expression, illumination and pose into account. Similarly, 2D-PCA for matrices has been used for feature extraction from face images without converting the images into vectors [20]. More recently, researchers have extended some of the manifold learning approaches from the vector case to tensors. He et al. [21] extended locality preserving projections [22] to second order tensors for face recognition. Dai and Yeung [23] presented generalized tensor embedding methods such as the extensions of local discriminant embedding methods [24], neighborhood preserving embedding methods [25], and locality preserving projection methods [22] to tensors. Li et al. [26] proposed a supervised manifold learning method for vector type data which preserves local structures in each class of samples, and then extended the algorithm to tensors to provide improved performance for face and gait recognition. Similar to vector-type manifold learning algorithms, the aim of these methods is to find an optimal *linear* transformation for the tensor-type data samples without vectorizing them and mapping these samples to a low dimensional subspace while preserving the neighbourhood information. However, these methods are mostly limited to supervised learning problems and cannot deal with unsupervised higher-order manifold learning problems.

In this paper, we propose a novel multiresoultion analysis technique to efficiently encode nonlinearities in tensor type data. The proposed method constructs data-dependent multiscale dictionaries to better represent the data. The proposed algorithm consists of two major steps: 1) Constructing a tree structure by decomposing the tensor into a collection of permuted subtensors, and 2) Constructing multiscale dictionaries by applying HoSVD to each subtensor. Finally, we apply the proposed algorithm to real datasets to illustrate the improvement in the compression performance compared to HoSVD. We introduce different variations of the proposed MS-HoSVD method including a single scale and multiple scale decomposition along with an adaptive pruning method. The computational complexity and memory requirements of the proposed method are given in comparison to conventional HoSVD. We also provide a theoretical error analysis for the proposed tensor partitioning approach in comparison to random partitioning.

It is important to note that the major contribution of this paper is to illustrate the use of this multiscale approach in data reduction and classification problems for general higher-order data. It is not our goal to simply introduce yet another new data compression or classification algorithm, but rather to demonstrate just a few applications of the novel multiscale approach proposed herein. In particular, we will show how the proposed method provides advantages over regular HoSVD when the data structure contains nonlinearities such as rotation or nonlinear distortion.

II. Background

A. Tensor Algebra

A multidimensional array with N modes $\mathscr{X} \in \mathbb{R}^{I_1 \times I_2 \times \ldots \times I_N}$ is called a tensor, where $x_{i_1,i_2,..i_N}$ denotes the $(i_1, i_2, ..i_N)^{th}$ element of the tensor $\mathscr{X}$. Vectors obtained by fixing all indices of the tensor except the one that corresponds to the nth mode are called mode-n fibers. Basic tensor operations are reviewed below [9], [27].

Mode-n product The mode-n product of a tensor $\mathscr{X} \in \mathbb{R}^{I_1 \times \ldots I_n \times \ldots \times I_N}$ and a matrix $\mathbf{U} \in \mathbb{R}^{J \times I_n}$ is denoted as $\mathscr{Y} = \mathscr{X} \times_n \mathbf{U}$, $(\mathscr{Y})_{i_1,i_2,\ldots,i_{n-1},j,i_{n+1},\ldots,i_N} = \sum_{i_n=1}^{I_n} x_{i_1,\ldots,i_n,\ldots,i_N} u_{j,i_n}$ and is of size $I_1 \times \ldots \times I_{n-1} \times J \times I_{n+1} \times \ldots \times I_N$.

Tensor matricization Process of reordering the elements of the tensor into a matrix is known as matricization or unfolding. The mode-n matricization of tensor $\mathscr{Y}$ is denoted as $\mathbf{Y}_{(n)}$ and is obtained by arranging mode-n fibers to be the columns of the resulting matrix. Unfolding the tensor $\mathscr{Y} = \mathscr{X} \times_1 \mathbf{U}^{(1)} \times_2 \mathbf{U}^{(2)} \ldots \times_N \mathbf{U}^{(N)}$ along mode-n is equivalent to $\mathbf{Y}_{(n)} = \mathbf{U}^{(n)} \mathbf{X}_{(n)} (\mathbf{U}^{(N)} \otimes \ldots \mathbf{U}^{(n+1)} \otimes \mathbf{U}^{(n-1)} \ldots \otimes \mathbf{U}^{(1)})^{\top}$, where $\otimes$ is the matrix Kronecker product.

Tensor Rank Unlike matrices, which have a unique definition of rank, there are multiple rank definitions for tensors including *tensor rank* and *tensor n-rank*. The *rank* of a tensor $\mathscr{X} \in \mathbb{R}^{I_1 \times \ldots I_n \times \ldots \times I_N}$ is the smallest number of rank-one tensors that form $\mathscr{X}$ as their sum. The *n-rank* of $\mathscr{X}$ is the collection of ranks of mode matrices $\mathbf{X}_{(n)}$ and is denoted as:

$$n\text{-rank}(\mathscr{X}) = \big(\text{rank}(\mathbf{X}_{(1)}), \text{rank}(\mathbf{X}_{(2)}), \ldots, \text{rank}(\mathbf{X}_{(N)})\big). \quad (1)$$

Tensor norm Norm of a tensor $\mathscr{X} \in \mathbb{R}^{I_1 \times I_2 \times \ldots \times I_N}$ is the square root of the sum of the squares of all its elements.

$$\| \mathscr{X} \| = \sqrt{\sum_{i_1=1}^{I_1} \sum_{i_2=1}^{I_2} \ldots \sum_{i_N=1}^{I_N} x_{i_1,i_2,\ldots,i_N}^2} \quad (2)$$

Tensor inner product The inner product of two same sized tensors $\mathscr{X}, \mathscr{Y} \in \mathbb{R}^{I_1 \times I_2 \times \ldots \times I_N}$ is the sum of the products of their elements.

$$\langle \mathscr{X}, \mathscr{Y} \rangle = \sum_{i_1=1}^{I_1} \sum_{i_2=1}^{I_2} \ldots \sum_{i_N=1}^{I_N} x_{i_1,i_2,\ldots,i_N} y_{i_1,i_2,\ldots,i_N} \tag{3}$$

B. Higher Order Singular Value Decomposition (HoSVD)

Any tensor $\mathscr{X} \in \mathbb{R}^{I_1 \times I_2 \times \ldots \times I_N}$ can be decomposed as mode products of a core tensor $\mathscr{S} \in \mathbb{R}^{I_1 \times I_2 \times \ldots \times I_N}$ with N orthogonal projection matrices $\mathbf{U}^{(n)} \in \mathbb{R}^{I_n \times I_n}$ each of which is composed of the left singular vectors of $\mathbf{X}_{(n)}$ [10]:

$$\mathscr{X} = \mathscr{S} \times_1 \mathbf{U}^{(1)} \times_2 \mathbf{U}^{(2)} \ldots \times_N \mathbf{U}^{(N)} = \mathscr{S} \times_{n=1}^{N} \mathbf{U}^{(n)} \tag{4}$$

where $\mathscr{S}$ is computed as

$$\mathscr{S} = \mathscr{X} \times_1 (\mathbf{U}^{(1)})^\top \times_2 (\mathbf{U}^{(2)})^\top \ldots \times_N (\mathbf{U}^{(N)})^\top. \tag{5}$$

Let $\mathscr{S}_{i_n=\alpha}$ be a subtensor of $\mathscr{S}$ obtained by fixing the nth index to α. This subtensor satisfies the following properties:

- all-orthogonality: $\mathscr{S}_{i_n=\alpha}$ and $\mathscr{S}_{i_n=\beta}$ are orthogonal for all possible values of n, α and β subject to $\alpha \neq \beta$.

$$\langle \mathscr{S}_{i_n=\alpha}, \mathscr{S}_{i_n=\beta} \rangle = 0 \; when \; \alpha \neq \beta. \tag{6}$$

- ordering:

$$\| \mathscr{S}_{i_n=1} \| \geq \| \mathscr{S}_{i_n=2} \| \geq \ldots \geq \| \mathscr{S}_{i_n=I_n} \| \geq 0 \tag{7}$$

for all possible values of n.

III. Multiscale Analysis of Higher-order Datasets

In this section, we present a new tensor decomposition method named Multiscale HoSVD (MS-HoSVD) for an Nth order tensor, $\mathscr{X} \in \mathbb{R}^{I_1 \times I_2 \times \ldots \times I_N}$. The proposed method recursively applies the following two-step approach: (i) Low-rank tensor approximation, (ii) Decomposing the residual (original minus low-rank) tensor into subtensors.

A tensor $\mathscr{X}$ is decomposed using HoSVD as follows:

$$\mathscr{X} = \mathscr{C} \times_1 \mathbf{U}^{(1)} \times_2 \mathbf{U}^{(2)} \ldots \times_N \mathbf{U}^{(N)}, \tag{8}$$

where the $\mathbf{U}^{(n)}$'s are the left singular vectors of the unfoldings $\mathbf{X}_{(n)}$. The low-rank approximation of $\mathscr{X}$ is obtained by

$$\hat{\mathscr{X}}_0 = \mathscr{C}_0 \times_1 \hat{\mathbf{U}}^{(1)} \times_2 \hat{\mathbf{U}}^{(2)} \ldots \times_N \hat{\mathbf{U}}^{(N)} \tag{9}$$

where $\hat{\mathbf{U}}^{(n)} \in \mathbb{R}^{I_n \times r_n}$s are the truncated projection matrices obtained by keeping the first r_n columns of $\mathbf{U}^{(n)}$ for all $n \in \{1, 2, \ldots, N\}$ and $\mathscr{C}_0 = \mathscr{X} \times_1 \hat{\mathbf{U}}^{(1),\top} \times_2 \hat{\mathbf{U}}^{(2),\top} \ldots \times_N \hat{\mathbf{U}}^{(N),\top}$. Multilinear-rank $\{r_1, \ldots, r_N\}$ can be given as a *priori* or an energy criterion can be used to determine the minimum number of singular values kept along each mode as:

$$r_n = arg \min_i \sum_{l=1}^{i} \lambda_l^{(n)} \quad s.t. \quad \frac{\sum_{l=1}^{i} \lambda_l^{(n)}}{\sum_{l=1}^{I_n} \lambda_l^{(n)}} > \tau, \tag{10}$$

where $\lambda_l^{(n)}$ is the lth singular value of the matrix obtained from the SVD of the unfolding $\mathbf{X}_{(n)}$, and τ is an energy threshold. Once $\hat{\mathscr{X}}_0$ is obtained, the tensor $\mathscr{X}$ can be written as

$$\mathscr{X} = \hat{\mathscr{X}}_0 + \mathscr{W}_0, \tag{11}$$

where $\mathscr{W}_0$ is the residual tensor.

For the first scale analysis, to better encode the details of $\mathscr{X}$, we adapted an idea similar to the one presented in [28], [29]. The 0th scale residual tensor, $\mathscr{W}_0$ is first decomposed into subtensors as follows. Tensor $\mathscr{W}_0 \in \mathbb{R}^{I_1 \times I_2 \times \ldots \times I_N}$ is unfolded across each mode yielding $\mathbf{W}_{0,(n)} \in \mathbb{R}^{I_n \times \prod_{j \neq n} I_j}$ whose columns are the mode-n fibers of $\mathscr{W}_0$. For each mode, rows of $\mathbf{W}_{0,(n)}$ are partitioned into c_n non-overlapping clusters using a clustering algorithm such as local subspace analysis (LSA) [30] . The Cartesian product of the partitioning labels coming from different modes yields index sets of $K = \prod_{i=1}^{N} c_i$ disjoint subtensors $\mathscr{X}_{1,k}$ where $k \in \{1, 2, \ldots, K\}$.

Let J_0^n be the index set corresponding to the nth mode of $\mathscr{W}_0$ where $J_0^n = \{1, 2, \ldots, I_n\}$, and $J_{1,k}^n$ be the index set of the subtensor $\mathscr{X}_{1,k}$ for the nth mode, where $J_{1,k}^n \subset J_0^n$ with $n \in \{1, 2, \ldots N\}$. Index sets of subtensors for the nth mode satisfy $\cup_{k=1}^{K} J_{1,k}^n = J_0^n$ for all $k, l \in \{1, 2, \ldots, K\}$. For example, the index set of the first subtensor $\mathscr{X}_{1,1}$ can be written as $J_{1,1}^1 \times J_{1,1}^2 \times \ldots \times J_{1,1}^N$ and the kth subtensor $\mathscr{X}_{1,k}$ is obtained by

$$\begin{gathered} \mathscr{X}_{1,k}(i_1, i_2, \ldots, i_N) = \mathscr{W}_0(J_{1,k}^1(i_1), J_{1,k}^2(i_2), \ldots, J_{1,k}^N(i_N)), \\ \mathscr{X}_{1,k} = \mathscr{W}_0(J_{1,k}^1 \times J_{1,k}^2 \times \ldots \times J_{1,k}^N), \end{gathered} \tag{12}$$

where $i_n \in \left\{1, 2, \ldots, J_{1,k}^n\right\}$. Low-rank approximation for each subtensor is obtained by applying HoSVD as:

$$\hat{\mathscr{X}}_{1,k} = \mathscr{C}_{1,k} \times_1 \hat{\mathbf{U}}_{1,k}^{(1)} \times_2 \hat{\mathbf{U}}_{1,k}^{(2)} \ldots \times_N \hat{\mathbf{U}}_{1,k}^{(N)}, \tag{13}$$

where $\mathscr{C}_{1,k}$ and $\hat{\mathbf{U}}_{1,k}^{(n)} \in \mathbb{R}^{|J_{1,k}^n| \times r_{1,k}^{(n)}}$s correspond to the core tensor and low-rank projection matrices of $\mathscr{X}_{1,k}$, respectively. $\hat{\mathscr{X}}_1$ is the 1st scale approximation of $\mathscr{X}$ formed by mapping all of the subtensors onto $\hat{\mathscr{X}}_{1,k}$ as follows:

$$\hat{\mathscr{X}}_1(J_{1,k}^1 \times J_{1,k}^2 \times \ldots \times J_{1,k}^n) = \hat{\mathscr{X}}_{1,k}. \tag{14}$$

Similarly, 1st scale residual tensor is obtained by

$$\mathscr{W}_1(J_{1,k}^1 \times J_{1,k}^2 \times \ldots \times J_{1,k}^n) = \mathscr{W}_{1,k}, \tag{15}$$

where $\mathscr{W}_{1,k} = \mathscr{X}_{1,k} - \hat{\mathscr{X}}_{1,k}$. Therefore, $\mathscr{X}$ can be rewritten as:

$$\mathscr{X} = \hat{\mathscr{X}}_0 + \mathscr{W}_0 = \hat{\mathscr{X}}_0 + \hat{\mathscr{X}}_1 + \mathscr{W}_1. \tag{16}$$

The jth scale approximation of $\mathscr{X}$ is obtained by decomposing $\mathscr{W}_{j-1,k}$s into subtensors $\mathscr{X}_{j,k}$s and fitting a low-rank model to each one of them in a similar fashion. Finally, the j^{th} scale decomposition of $\mathscr{X}$ can be written as:

$$\mathscr{X} = \sum_{i=0}^{j} \hat{\mathscr{X}}_i + \mathscr{W}_j. \tag{17}$$

See Algorithm 1 for pseudo code describing this approach.

A. Memory Cost of the First Scale Decomposition

Let $\mathscr{X} \in \mathbb{R}^{I_1 \times I_2 \times \ldots \times I_N}$ be an Nth order tensor. To simplify the notation, assume that the dimension of each mode is the same, i.e. $I_1 = I_2 = \ldots = I_N = I$. Assume $\mathscr{X}$ is approximated by HoSVD as:

$$\hat{\mathscr{X}} = \mathscr{C}_H \times_1 \mathbf{U}_H^{(1)} \times_2 \mathbf{U}_H^{(2)} \ldots \times_N \mathbf{U}_H^{(N)}, \tag{18}$$

Algorithm 1 Multiscale HoSVD

Input: $\mathscr{X}$: tensor , $\mathbf{C} = (c_1, c_2, ..., c_N)$: the desired number of clusters for each mode, s_H: the highest scale of MS-HoSVD.
Output: T: Tree structure containing the MS-HoSVD decomposition of $\hat{\mathscr{X}}$.
Create an empty tree T
Create an empty list L
Add the node containing $\mathscr{X}$ to L.
while L is not empty. **do**
    Select a node corresponding to $\mathscr{X}_{s,t}$ (the tth subtensor from sth scale) from the list L where $s \in \{0, ..., s_H\}$ and $t \in \{1, ..., K^s\}$.
    $\mathscr{C}_{s,t}, \left\{\hat{\mathbf{U}}_{s,t}^{(n)}\right\} \leftarrow$ truncatedHOSVD($\mathscr{X}_{s,t}$).
    Add the node containing $\mathscr{C}_{s,t}, \left\{\hat{\mathbf{U}}_{s,t}^{(n)}\right\}$ to T.
    if $s < s_H$ **then**
        Compute $\mathscr{W}_{s,t} = \mathscr{X}_{s,t} - \hat{\mathscr{X}}_{s,t}$.
        Create K subtensors $\mathscr{X}_{s+1,K(t-1)+k}$ with $J^n_{s+1,K(t-1)+k}$ from $\mathscr{W}_{s,t}$ where $k \in \{1, 2, ..., K\}$ and $n \in \{1, 2, ..., N\}$.
        Add K nodes containing $\mathscr{X}_{s+1,K(t-1)+k}$ and $\left\{J^n_{s+1,K(t-1)+k}\right\}$ to L.
    end if
end while

by fixing the rank of each mode matrix as $\text{rank}(\mathbf{U}_H^{(i)}) = r_H$ for $i \in \{1, 2, ..., N\}$. Let $\mathbb{F}(\cdot)$ be a function that quantifies the memory cost, then the storage cost of $\mathscr{X}$ decomposed by HoSVD is $\mathbb{F}(\mathscr{C}_H) + \sum_{i=1}^N (\mathbb{F}(\mathbf{U}_H^{(i)})) \approx r_H^N + NIr_H$.

For multiscale analysis at scale 1, $\mathscr{X} = \hat{\mathscr{X}}_0 + \hat{\mathscr{X}}_1$. The cost of storing $\hat{\mathscr{X}}_0$ is $\mathbb{F}(\mathscr{C}_0) + \sum_{i=1}^N (\mathbb{F}(\hat{\mathbf{U}}^{(i)})) \approx r_0^N + NIr_0$ where the rank of each mode matrix is fixed at $\text{rank}(\mathbf{U}^{(i)}) = r_0$ for $i \in \{1, 2, ..., N\}$. The cost of storing $\hat{\mathscr{X}}_1$ is the sum of the storage costs for each of the $K = \prod_{i=1}^N c(i)$ subtensors $\hat{\mathscr{X}}_{1,k}$. Assume $c(i) = c$ for all $i \in \{1, 2, ..., N\}$ yielding c^N equally sized subtensors, and that each $\hat{\mathscr{X}}_{1,k}$ is decomposed using the HoSVD as $\hat{\mathscr{X}}_{1,k} = \mathscr{C}_{1,k} \times_1 \hat{\mathbf{U}}_{1,k}^{(1)} \times_2 \hat{\mathbf{U}}_{1,k}^{(2)} ... \times_N \hat{\mathbf{U}}_{1,k}^{(N)}$. Let the rank of each mode matrix be fixed as $\text{rank}(\hat{\mathbf{U}}_{1,k}^{(i)}) = r_1$ for all $i \in \{1, 2, ..., N\}$ and $k \in \{1, 2, ..., K\}$. Then, the memory cost for the first scale is $\sum_{k=1}^K (\mathbb{F}(\mathscr{C}_{1,k}) + \sum_{i=1}^N \mathbb{F}(\hat{\mathbf{U}}_{1,k}^{(i)})) \approx c^N (r_1^N + \frac{NIr_1}{c})$. Choosing $r_1 \lesssim \frac{r_0}{c^{(N-1)}}$ ensures that the storage cost does not grow exponentially so that $\mathbb{F}(\hat{\mathscr{X}}_1) < \mathbb{F}(\hat{\mathscr{X}}_0)$ since the total cost becomes approximately equal to $r_0^N (1 + \frac{1}{c^{N^2-2N}}) + 2NIr_0$. Thus, picking $r_0 \approx r_H/2$ can now provide lower storage cost for the first scale analysis than for HoSVD.

B. Computational Complexity

Computational complexity of HoSVD of an N-way tensor $\mathscr{X} \in \mathbb{R}^{I_1 \times I_2 \times ... \times I_N}$ where $I_1 = I_2 = ... = I_N = I$ is $O\left(I^{(N+1)}\right)$ [31]. By assuming that the clustering is performed using K-means with $c_i = c$ along each mode, the complexity of first scale MS-HoSVD analysis due to clustering along each mode is, $O\left(NI^N ci\right)$, where i is the number of iterations. Moreover, the total complexity of applying the HoSVD to c^N equally sized subtensors is $O\left(c^N (I/c)^{(N+1)}\right)$. Therefore, first scale MS-HoSVD has computational complexity of $O\left(I^{(N+1)} + NI^N ci + c^N (I/c)^{(N+1)}\right)$. Note that this complexity is similar to that of the HoSVD whenever Nci is small compared to I. Of course, the runtime complexity of these multiscale methods can be reduced even further by, e.g., computing the HoSVDs for different subtensors in parallel whenever possible, as well as by utilizing distributed and parallel SVD algorithms such as [32] when computing all the required HoSVD decompositions.

IV. Near-Optimal Partitioning, and Error Analysis

A. Definitions

For an N-way tensor $\mathscr{X} \in \mathbb{R}^{I_1 \times I_2 \times ... I_N}$ disjoint subtensors $\mathscr{X}|_k$ can also be formed using diagonal restriction matrices $\mathbf{R}_k^{(n)} \in \{0, 1\}^{I_n \times I_n}$ by setting

$$\mathscr{X}|_k := \mathscr{X} \times_1 \mathbf{R}_k^{(1)} \times_2 \mathbf{R}_k^{(2)} ... \times_N \mathbf{R}_k^{(N)}, \tag{19}$$

where $\mathbf{R}_k^{(n)}(i,j) = \begin{cases} 1, & \text{if } i = j \text{ and } j \in J^n_{1,k} \\ 0, & \text{otherwise} \end{cases}$ for $k \in \{1, 2, ..., K\}$. Thus, the kth subtensor $\mathscr{X}|_k$ will only have nonzero entries, given by $\mathscr{X}(J^1_{1,k} \times ... \times J^N_{1,k})$, in the locations indexed by the sets $J^n_{1,k}$ from the last section. Note that the dimensionality of the subtensors defined in this way are the same as the original tensor so that $\mathscr{X}|_k \in \mathbb{R}^{I_1 \times I_2 \times ... I_N}$ for all k. As a result, this new definition allows us to do algebraic operations with subtensors across different scales so that, e.g., $\hat{\mathscr{X}}_0 + \hat{\mathscr{X}}_1|_k$ now makes sense for all k. Finally, in this section all the restriction matrices $\mathbf{R}$ and projection matrices $\mathbf{P}$ with or without a symbol on top of them will be low-rank.

B. Characterizing Low-Rank Subtensors

Given $\mathscr{X} \in \mathbb{R}^{I_1 \times I_2 \times ... I_N}$ and restriction matrices $\mathbf{R}_k^{(n)}$, let $\mathbf{Q}_k^{(n)} \in \mathbb{R}^{I_n \times I_n}$ be the mode-n projection operator corresponding to $\mathbf{Q}_k^{(n)} = \mathbf{U}_k^{(n)} (\mathbf{U}_k^{(n)})^\top$ where $\mathbf{U}_k^{(n)}$ is the nth mode orthogonal matrix of rank $\leq rank(\mathbf{R}_k^{(n)})$ obtained from the truncated HoSVD of the subtensor $\mathscr{X} \times_{n=1}^N \mathbf{R}_k^{(n)}$. Now let each $\mathbf{P}_k^{(n)}$ be $\mathbf{Q}_k^{(n)}$ with its rows and columns permuted so that $\mathbf{P}_k^{(n)} \mathbf{R}_k^{(n)} = \mathbf{P}_k^{(n)} = \mathbf{R}_k^{(n)} \mathbf{P}_k^{(n)}$ holds for all n. Using this notation $\mathscr{X} = \sum_{k=1}^K \mathscr{X}|_k$ can be approximated as the sum of low-rank approximations of its subtensors by

$$\mathscr{X} \approx \sum_{k=1}^K \mathscr{X} \times_{n=1}^N \mathbf{R}_k^{(n)} \mathbf{P}_k^{(n)} = \sum_{k=1}^K \mathscr{X} \times_{n=1}^N \mathbf{P}_k^{(n)}. \tag{20}$$

In order to provide an error bound for 1-scale MS-HoSVD similar to the error bound of truncated HoSVD as in [33], we define optimal and pessimistic partitions as follows. Let the restriction matrices $\left\{\hat{\mathbf{R}}_k^{(n)}\right\}$ form a partition of $\mathscr{X}$ yielding low-rank projection matrices $\left\{\hat{\mathbf{P}}_k^{(n)}\right\}$ and rank-$(\hat{r}_1, ...\hat{r}_N)$ approximations of $\mathscr{X}|_k$ for each $k \in \{1, ..K\}$ as per (20). The partition formed by the $\left\{\hat{\mathbf{R}}_k^{(n)}\right\}$ restriction matrices will be called *near-optimal* if there exists another set of *pessimistic* partitioning restriction matrices $\left\{\tilde{\mathbf{R}}_k^{(n)}\right\}$ together with a bijection $f : [K] \to [K]$ that satisfy

$$\sum_{n=1}^N \left|\left| \mathscr{X}|_k \times_n (\hat{\mathbf{R}}_k^{(n)} - \hat{\mathbf{P}}_k^{(n)}) \right|\right|^2 \leq \sum_{n=1}^N \left|\left| \mathscr{X} \times_n \tilde{\mathbf{R}}_{f(k)}^{(n)} (\mathbf{I} - \bar{\mathbf{P}}_n) \times_{l \neq n}^N \tilde{\mathbf{R}}_{f(k)}^{(l)} \right|\right|^2 \tag{21}$$

for each $k \in \{1,..K\}$. In eqn. (21) the $\left\{\bar{\mathbf{P}}_k^{(n)}\right\}$ are projections obtained from the truncated HoSVD of $\mathscr{X}$ with ranks $\bar{r}_n \geq \hat{r}_n \ \forall n$.

Remark 1: Optimal partitions satisfying (21) certainly exist for some tensors. For example, consider a 3-mode tensor $\mathscr{X} \in \mathbb{R}^{I\times I\times I}$ formed by 8 orthogonal $(1,\,1,\,1)$-rank 3-way subtensors of equal size. The ground truth partitions' restriction matrices $\left\{\hat{\mathbf{R}}_k^{(n)}\right\}$ lead to rank 1 projection matrices $\left\{\hat{\mathbf{P}}_k^{(n)}\right\}$ producing zero error, $\sum_{n=1}^{3}\left|\left|\mathscr{X}|_k \times_n (\hat{\mathbf{R}}_k^{(n)} - \hat{\mathbf{P}}_k^{(n)})\right|\right|^2 = 0$, for all $k \in \{1,\ldots,8\}$. If we now exchange even a single non-zero row of $\hat{\mathbf{R}}_1^{(n)}$ with a nonzero row of $\hat{\mathbf{R}}_2^{(n)}$ yielding a new set of pessimistic matrices $\left\{\tilde{\mathbf{R}}_k^{(n)}\right\}$ different than the true partition, then the rank 1 projection matrices $\left\{\bar{\mathbf{P}}_k^{(n)}\right\}$s will produce a nonzero error for the right hand side of eqn. (21) whenever, e.g., $k = 1,2$.

Remark 2: Though choosing subtensors via subspace clustering may not produce ground truth partitions in more complicated mixed rank situations, experiments indicate that the found subtensors do still perform significantly better than, e.g., randomly partitioning into subtensors (and, therefore, worst case subtensor partitioning). In what follows we will demonstrate this fact with several experiments. The experiments will also demonstrate that partitions satisfying eqn. (21) not only exist, but are commonly found via subspace clustering.

1) Experiment-1: In this experiment, a three-way tensor $\mathscr{X} \in \mathbb{R}^{20\times 20\times 20}$ is formed by concatenating 8 subtensors $\mathscr{X}_k \in \mathbb{R}^{10\times 10\times 10}$s of multilinear-rank $\{2,\,2,\,2\}$. Low-rank approximations for $\mathscr{X}$ are obtained by applying truncated HoSVD to $\mathscr{X}$ as well as to the ground truth partitions $\mathbf{R}_k^{(n)}$, partitions provided by a clustering algorithm $\hat{\mathbf{R}}_k^{(n)}$ and random partitions $\tilde{\mathbf{R}}_k^{(n)}$. Clustering is performed by local subspace analysis (LSA) [30] and cluster numbers are selected as 2 along each mode yielding 8 subtensors. Normalized reconstruction error is computed over 20 trials for varying multilinear rank as $\frac{\|\mathscr{X}-\hat{\mathscr{X}}\|_F}{\|\mathscr{X}\|_F}$ where $\hat{\mathscr{X}}$ is an approximation of $\mathscr{X}$.

As expected, using a clustering algorithm provides lower rank subtensors than using random partitions, however, those subtensors are not as low-rank as the ones obtained from the ground truth partitions. Morever, it can also be seen that obtaining a low-rank approximation to $\mathscr{X}$ using truncated HoSVD is not very accurate and leads to high reconstruction error (see Table I).

Moreover, to verify that eqn. (21) indeed holds, the left (LHS) and right (RHS) hand sides in eqn. (21) for each subtensor are computed where optimum partitions $\hat{\mathbf{P}}_k^{(n)}$s are obtained from ground truth partitioning and clustering with $\hat{r}_n = 2$ separately, $\bar{\mathbf{P}}^{(n)}$s are obtained from truncated HoSVD with varying ranks as $\bar{r}_n = \kappa\hat{r}_n$ with $\kappa \in \{1,\,2\,,3\}$, and $\tilde{\mathbf{R}}_k^{(n)}$s are generated randomly. In Table II, we report mean value and standard deviation of the minimum gap of RHS - LHS, for a bijection satisfying eqn. (21). As seen in Table II, RHS of eqn. (21) yields higher error for $\bar{\mathbf{P}}^{(n)}$s with varying ranks compared to LHS with $\hat{\mathbf{P}}_k^{(n)}$ obtained from both ground truth partitioning and clustering.

TABLE I: Mean and standard deviation for normalized reconstruction error for low-rank approximations of $\mathscr{X}$ containing simulated data over 20 trial.

	Reconstruction Error		
$(\hat{r}_1,\,\hat{r}_2,\,\hat{r}_3)$	(2, 2, 2)	(4, 4, 4)	(6, 6, 6)
Ground Truth Partitioning	0.8087e-015 ± 0.1101e-016	- -	- -
Clustering by LSA	0.2141 ± 0.1644	0.0419 ± 0.0552	0.0066 ± 0.0219
$(\tilde{r}_1,\,\tilde{r}_2,\,\tilde{r}_3)$	(2, 2, 2)	(4, 4, 4)	(6, 6, 6)
Random Partitioning	0.7916 ±0.0330	0.5642 ±0.0448	0.3506 ± 0.0362
$(\bar{r}_1,\,\bar{r}_2,\,\bar{r}_3)$	(4, 4, 4)	(8, 8, 8)	(12, 12, 12)
truncated HoSVD	0.7743 ±0.0428	0.4579 ± 0.0437	0.1851 ± 0.0304

TABLE II: Verification of eqn. (21) (mean and std.) for simulated data over 20 trials.

	RHS - LHS in eqn. (21)		
$(\bar{r}_1,\bar{r}_2,\bar{r}_3)$	(2, 2, 2)	(4, 4, 4)	(6, 6, 6)
Ground Truth Partitioning with $(\hat{r}_1,\hat{r}_2,\hat{r}_3) = (2,\,2,\,2)$	9.9666 ±2.9103	6.2890 ±1.6121	5.6757 ±1.2644
Clustering by LSA with $(\hat{r}_1,\hat{r}_2,\hat{r}_3) = (2,\,2,\,2)$	9.8374 ±2.8648	5.3452 ±1.7007	4.8957 ±1.5375

2) Experiment-2: In this experiment, we performed similar steps as in *Experiment-1* on a three-mode tensor $\mathscr{X} \in \mathbb{R}^{244\times 320\times 138}$ containing PIE dataset (see Section VI-A2 for more details). Low-rank approximation for $\mathscr{X}$ is obtained by applying truncated HoSVD to the subtensors of $\mathscr{X}$ determined by restrictions matrices $\hat{\mathbf{R}}_k^{(n)}$ obtained from clustering along each mode. Clustering is performed by LSA and cluster numbers are selected as 2 along each mode yielding 8 subtensors. The $(\hat{r}_1,\,\hat{r}_2,\,\hat{r}_3)$-rank used in truncated HoSVD of subtensors are selected adaptively using the energy criterion as described in Section III. τ is tuned empirically to provide 5 percent reconstruction error for $\mathscr{X}$ and the same τ is used for all low-rank subtensor approximations yielding different multilinear-ranks for each subtensor as $(\hat{r}_1,\,\hat{r}_2,\,\hat{r}_3)_k$. $(\bar{r}_1,\,\bar{r}_2,\,\bar{r}_3)$-rank used in truncated HoSVD of $\mathscr{X}$ and $(\tilde{r}_1,\,\tilde{r}_2,\,\tilde{r}_3)$-rank used in truncated HoSVD of the subtensors obtained by random partitioning are selected as the average of $(\hat{r}_1,\,\hat{r}_2,\,\hat{r}_3)_k$ across subtensors and are increased gradually by multiplying with a constant $\kappa \in \{1,\,1.50\,,1.75\}$.

Average multilinear rank across subtensors obtained by clustering is computed as $(35,\,43,\,17)$ and reconstruction errors for fitting low-rank model to the subtensors obtained by both clustering and random partitions are given in Table III. Similar to *Experiments-1*, using a clustering algorithm provides lower rank subtensors than using random partitions. Morever, it can also be seen that rank of the low-rank approximation to $\mathscr{X}$ obtained by truncated HoSVD is not as low as fitting low-rank model to subtensors coming from clustering and random partitioning.

In order to provide a real data example satisfying eqn. (21), left (LHS) and and right (RHS) sides in eqn. (21) for each subtensor are computed where optimum partitions $\hat{\mathbf{P}}_k^{(n)}$s are obtained from clustering, $\bar{\mathbf{P}}^{(n)}$s obtained from truncated

TABLE III: Mean and standard deviation for $\{r_n\}$ for low-rank approximations of $\mathscr{X}$ containing PIE data over 20 trial.

	Reconstruction Error		
$(\hat{r}_1,\ \hat{r}_2,\ \hat{r}_3)$	(35, 43, 17)		
Clustering by LSA	0.0491 -		
$(\bar{r}_1,\ \bar{r}_2,\ \bar{r}_3)$	(35, 43, 17)	(53, 65, 26)	(61, 75, 30)
Random Partitioning	0.0900 ± 8.9087e-4	0.0604 ±7.9251e-4	0.0510 ±5.5432e-4
$(\bar{r}_1,\ \bar{r}_2,\ \bar{r}_3)$	(35, 43, 17)	(53, 65, 26)	(61, 75, 30)
truncated HoSVD	0.1023 ± 1.4238e-17	0.0748 ± 2.8477e-17	0.0666 ± 1.4238e-17

TABLE IV: Verification of eqn. (21) (mean and std.) for PIE data over 20 trials.

	RHS - LHS in eqn. (21)		
$(\bar{r}_1,\ \bar{r}_2,\ \bar{r}_3)$	(35, 43, 17)	(53, 65, 26)	(61, 75, 30)
Clustering by LSA with $(\hat{r}_1,\hat{r}_2,\hat{r}_3) = (35, 43, 17)$	0.0090 ± 4.4524e-4	0.0019 ± 3.6879e-4	0.0003 ± 2.2691e-4

HoSVD with varying ranks as $(\bar{r}_1,\ \bar{r}_2,\ \bar{r}_3) = \kappa(35,\ 43,\ 17)$ with $\kappa \in \{1,\ 1.50\ , 1.75\}$, and $\tilde{\mathbf{R}}_k^{(n)}$s are selected randomly. In Table IV, we reported mean value and standard deviation of the minimum gap between RHS and LHS for a bijection satisfying eqn. (21) similar to previous experiment. As seen in Table IV, RHS of eqn. (21) yields higher error for $\bar{\mathbf{P}}^{(n)}$s even with a high rank compared to LHS with $\hat{\mathbf{P}}_k^{(n)}$ obtained from clustering.

3) Experiment-3: In this experiment, we evaluated the error obtained by 1st scale MS-HoSVD analysis of a tensor similar to the model described in Section III. A three-way tensor $\mathscr{X} \in \mathbb{R}^{20\times20\times20}$ is the sum of two tensors as $\mathscr{X} = \mathscr{X}_0 + \mathscr{X}_1$ where $\mathscr{X}_0 \in \mathbb{R}^{20\times20\times20}$ is of multilinear rank $\{2,\ 2,\ 2\}$ and $\mathscr{X}_1 \in \mathbb{R}^{20\times20\times20}$ is formed by concatenating 8 subtensors $\mathscr{X}_k \in \mathbb{R}^{10\times10\times10}$ of multilinear-rank $\{2,\ 2,\ 2\}$. Low-rank approximations for $\mathscr{X}$ are obtained by applying truncated HoSVD to $\mathscr{X}$ and using 1-scale MS-HoSVD to the ground truth partitions $\mathbf{R}_k^{(n)}$, partitions provided by a clustering algorithm $\hat{\mathbf{R}}_k^{(n)}$ and random partitions $\tilde{\mathbf{R}}_k^{(n)}$. Clustering is performed by LSA and cluster numbers are selected as 2 along each mode yielding 8 subtensors. 0th scale multilinear rank for MS-HoSVD is selected as $\{2,\ 2,\ 2\}$ and varying 1st scale ranks are used in the experiments as shown in Table V. Normalized reconstruction error computed for varying multilinear rank can be seen in Table V. Similar to previous experiments, using ground truth partition provides lower-rank subtensors and using clustering leads to much better approximation than HoSVD.

Similar to the previous experiments, LHS and RHS in eqn. (21) for each subtensor belonging to the 1st scale MS-HOSVD approximation are computed where optimum partitions $\hat{\mathbf{P}}_k^{(n)}$s are obtained from ground truth partitioning and clustering with $\hat{r}_n = 4$ separately and $\bar{\mathbf{P}}^{(n)}$s are obtained from truncated HoSVD of $\mathscr{W}_0$ with varying ranks as $\bar{r}_n = \kappa\hat{r}_n$ with $\kappa \in \{1,\ 1.5\ , 2\}$, and $\tilde{\mathbf{R}}_k^{(n)}$s are selected randomly. In Table VI, we reported mean value and standard deviation of the minimum gap between RHS and LHS of the bijection satisfying eqn. (21). As seen in Table VI, eqn. (21) also holds for 1st scale approximation of MS-HoSVD and RHS of eqn. (21) leads to higher error for $\bar{\mathbf{P}}^{(n)}$s compared to LHS with $\hat{\mathbf{P}}_k^{(n)}$s obtained from both ground truth partitioning and clustering.

TABLE V: Mean and standard deviation for reconstruction error of low-rank approximations of $\mathscr{X}$ over 20 trial.

	Reconstruction Error		
1st scale rank	{2, 2, 2}	{4, 4, 4}	{6, 6, 6}
Ground Truth Partitioning	0.3481 ± 0.0497	0.1079 ± 0.0199	0.1122e-014 0.0200e-014
Clustering by LSA	0.5089 ± 0.0804	0.2797 ± 0.0940	0.1458 ± 0.0492
Random Partitioning	0.7624 ± 0.0327	0.5822 ± 0.0343	0.3772 ± 0.0325
rank	{4, 4, 4}	{8, 8, 8}	{12, 12, 12}
truncated HoSVD	0.8014 ±0.0431	0.4975 ± 0.0256	0.2304 ± 0.0269

TABLE VI: Verification of eqn. (21) (mean and std.) for simulated data over 20 trials.

	RHS - LHS in eqn. (21)		
$(\bar{r}_1,\bar{r}_2,\bar{r}_3)$	(4, 4, 4)	(6, 6, 6)	(8, 8, 8)
Ground Truth Partitioning with $(\hat{r}_1,\hat{r}_2,\hat{r}_3) = (4,\ 4,\ 4)$	2.2892 ± 0.6702	0.8409 ± 0.2173	0.3749 ± 0.0946
Clustering by LSA with $(\hat{r}_1,\hat{r}_2,\hat{r}_3) = (4,\ 4,\ 4)$	2.2538 ± 0.6539	0.7854 ± 0.2781	0.1218 ± 0.2901

C. A Theoretical Error Bound

Lemma 1: Let $\mathscr{X} \in \mathbb{R}^{I_1\times I_2\times\ldots I_N}$ and $\left\{\hat{\mathbf{R}}_k^{(n)}\right\}$ be a collection of restrictions that form a near-optimal partition of $\mathscr{X}$ with respect to a pessimistic partition formed via $\tilde{R}_k^{(n)}$ as per eqn. (21). Let $\bar{\mathbf{P}}^{(n)}$ be the rank $\bar{r}_n \geq \hat{r}_n$ projection matrix from eqn. (21) obtained via the truncated HoSVD of $\mathscr{X}$. Then

$$\left|\left|\mathscr{X} - \sum_{k=1}^{K} \mathscr{X}|_k \times_{n=1}^{N} \hat{\mathbf{P}}_k^{(n)}\right|\right|^2 \leq \sum_{n=1}^{N} \left|\left|\mathscr{X} \times_n (\mathbf{I} - \bar{\mathbf{P}}^{(n)})\right|\right|^2. \quad (22)$$

Proof:

$$\begin{aligned} \left|\left|\mathscr{X} - \textstyle\sum_{k=1}^{K} \mathscr{X}|_k \times_{n=1}^{N} \hat{\mathbf{P}}_k^{(n)}\right|\right|^2 &= \left|\left|\textstyle\sum_{k=1}^{K} \mathscr{X} \times_{n=1}^{N} \hat{\mathbf{R}}_k^{(n)} - \sum_{k=1}^{K} \mathscr{X}|_k \times_{n=1}^{N} \hat{\mathbf{P}}_k^{(n)}\right|\right|^2 \\ &= \left|\left|\textstyle\sum_{k=1}^{K} \left(\mathscr{X} \times_{n=1}^{N} \hat{\mathbf{R}}_k^{(n)} - \mathscr{X}|_k \times_{n=1}^{N} \hat{\mathbf{P}}_k^{(n)}\right)\right|\right|^2 \\ &= \textstyle\sum_{k=1}^{K} \left|\left|\mathscr{X} \times_{n=1}^{N} \hat{\mathbf{R}}_k^{(n)} - \mathscr{X}|_k \times_{n=1}^{N} \hat{\mathbf{P}}_k^{(n)}\right|\right|^2 \end{aligned} \quad (23)$$

By using theorem 5.1 from [33], we can rewrite eqn. (23):

$$\begin{aligned} \text{Eqn. (23)} = &\ \textstyle\sum_{k=1}^{K}\sum_{h=1}^{N} \left|\left|\mathscr{X} \times_h (\hat{\mathbf{R}}_k^{(h)} - \hat{\mathbf{P}}_k^{(h)}) \times_{l=1}^{h-1} \hat{\mathbf{P}}_k^{(l)} \times_{l=h+1}^{N} \hat{\mathbf{R}}_k^{(l)}\right|\right|^2 \\ \leq &\ \textstyle\sum_{k=1}^{K}\sum_{h=1}^{N} \left|\left|\mathscr{X} \times_h (\hat{\mathbf{R}}_k^{(h)} - \hat{\mathbf{P}}_k^{(h)}) \times_{l\neq h}^{N} \hat{\mathbf{R}}_k^{(l)}\right|\right|^2. \end{aligned} \quad (24)$$

By using the definition in eqn (21):

$$\begin{aligned} \text{Eqn. (24)} \leq &\ \textstyle\sum_{k=1}^{K}\sum_{h=1}^{N} \left|\left|\mathscr{X} \times_h \tilde{\mathbf{R}}_k^{(h)} (\mathbf{I} - \bar{\mathbf{P}}^{(h)}) \times_{l\neq h}^{N} \tilde{\mathbf{R}}_k^{(l)}\right|\right|^2 \\ = &\ \textstyle\sum_{h=1}^{N} \left|\left|\mathscr{X} \times_h (\mathbf{I} - \bar{\mathbf{P}}^{(h)})\right|\right|^2 \quad \blacksquare \end{aligned} \quad (25)$$

Lemma 1 indicates that the error in approximating $\mathscr{X}$ via low-rank approximations of its near-optimal subtensors is smaller than the error obtained by approximating $\mathscr{X}$ via (potentially higher rank) truncated HoSVDs [33].

Theorem 1: For an Nth order tensor $\mathscr{X} \in \mathbb{R}^{I_1 \times I_2 \ldots \times I_N}$, first scale approximation error given by MS-HoSVD is bounded by:

$$\begin{aligned} ||\mathscr{X} - \hat{\mathscr{X}_0} - \hat{\mathscr{X}_1}||^2 \leq \quad & \Sigma_{h=1}^{N} \left|\left| \mathscr{X} \times_h (\mathbf{I} - \bar{\mathbf{P}}^{(h)}) \right|\right|^2 \\ & + \Sigma_{h=1}^{N} \Sigma_{n=1}^{h-1} \left|\left| \mathscr{X} \times_h (\mathbf{I} - \bar{\mathbf{P}}^{(h)}) \times_n (\mathbf{I} - \mathbf{P}^{(n)}) \right|\right|^2 \end{aligned} \tag{26}$$

where $\left\{\bar{\mathbf{P}}^{(h)}\right\}$ are low-rank projection matrices of rank $\bar{r}_n$ obtained by truncated HoSVD for $\mathscr{X}$ as per eqn. (21), and $\left\{\mathbf{P}^{(n)}\right\}$ are r_n-rank projection matrices for $\mathscr{X}_0$ with $r_n \leq \bar{r}_n$ for all n.

Proof: Using Lemma 1, $\left|\left|\mathscr{X} - \hat{\mathscr{X}_0} - \hat{\mathscr{X}_1}\right|\right|^2$ can be bounded as follows:

$$\begin{aligned} ||\mathscr{X} - \hat{\mathscr{X}_0} - \hat{\mathscr{X}_1}||^2 \leq \quad & \Sigma_{h=1}^{N} \left|\left| (\mathscr{X} - \mathscr{X}_0) \times_h (\mathbf{I} - \bar{\mathbf{P}}^{(h)}) \right|\right|^2 \\ = \quad & \Sigma_{h=1}^{N} \left|\left| \left(\mathscr{X} - \mathscr{X} \times_{j=1}^{N} \mathbf{P}^{(j)}\right) \times_h (\mathbf{I} - \bar{\mathbf{P}}^{(h)}) \right|\right|^2 \end{aligned} \tag{27}$$

By using (5.2) from the proof of theorem 5.1 in [33]:

$$\begin{aligned} \text{Eqn. (27)} = \quad & \Sigma_{h=1}^{N} \left|\left| \left(\Sigma_{n=1}^{N} \mathscr{X} \times_n (\mathbf{I} - \mathbf{P}^{(n)}) \times_{l=1}^{n-1} \mathbf{P}^{(l)}\right) \times_h (\mathbf{I} - \bar{\mathbf{P}}^{(h)}) \right|\right|^2 \\ = \quad & \Sigma_{h=1}^{N} \left|\left| \left(\Sigma_{n=1}^{h-1} \mathscr{X} \times_n (\mathbf{I} - \mathbf{P}^{(n)}) \times_{l=1}^{n-1} \mathbf{P}^{(l)}\right) \times_h (\mathbf{I} - \bar{\mathbf{P}}^{(h)}) \right.\right. \\ & \left.\left. + \ \mathscr{X} \times_h (\mathbf{I} - \bar{\mathbf{P}}^{(h)}) (\mathbf{I} - \mathbf{P}^{(h)}) \times_{l=1}^{h-1} \mathbf{P}^{(l)} \right|\right|^2 \end{aligned} \tag{28}$$

Since both $\mathbf{P}^{(n)}$ and $\bar{\mathbf{P}}^{(n)}$ are obtained from SVD of the nth-mode unfolded matrix of $\mathscr{X}$, the column space of $\bar{\mathbf{P}}^{(n)}$ contains the column space of $\mathbf{P}^{(n)}$ yielding $(\mathbf{I} - \bar{\mathbf{P}}^{(h)})(\mathbf{I} - \mathbf{P}^{(h)}) = (\mathbf{I} - \bar{\mathbf{P}}^{(h)})$. Therefore,

$$\begin{aligned} \text{Eqn. (28)} = \quad & \Sigma_{h=1}^{N} \left|\left| \left(\Sigma_{n=1}^{h-1} \mathscr{X} \times_n (\mathbf{I} - \mathbf{P}^{(n)}) \times_{l=1}^{n-1} \mathbf{P}^{(l)}\right) \times_h (\mathbf{I} - \bar{\mathbf{P}}^{(h)}) \right|\right|^2 \\ & + \Sigma_{h=1}^{N} \left|\left| \mathscr{X} \times_h (\mathbf{I} - \bar{\mathbf{P}}^{(h)}) \times_{l=1}^{h-1} \mathbf{P}^{(l)} \right|\right|^2 \\ \leq \quad & \Sigma_{h=1}^{N} \left|\left| \mathscr{X} \times_h (\mathbf{I} - \bar{\mathbf{P}}^{(h)}) \right|\right|^2 \\ & + \Sigma_{h=1}^{N} \Sigma_{n=1}^{h-1} \left|\left| \mathscr{X} \times_h (\mathbf{I} - \bar{\mathbf{P}}^{(h)}) \times_n (\mathbf{I} - \mathbf{P}^{(n)}) \right|\right|^2 \quad \blacksquare \end{aligned} \tag{29}$$

V. Tree Pruning in Multiscale HoSVD

In order to better capture the local structure of the tensor, it is important to look at higher scale decompositions. However, as the scale increases, the storage cost and computational complexity will increase making any gain in reconstruction error not worth the additional memory cost. For this reason, it is important to carefully select the subtensors adaptively at higher scales. To identify the suboptimal decomposition structure, we propose an adaptive pruning method across scales.

In adaptive pruning, the tree is pruned by minimizing the following cost function $\mathbb{H} = Error + \eta \cdot Compression$ similar to the rate-distortion criterion commonly used by compression algorithms where η is the trade-off parameter [34]. To minimize this function we apply a procedure similar to sequential forward selection [35]. First, the root node which stores $\hat{\mathscr{X}_0}$ is created and scale-1 subtensors $\hat{\mathscr{X}_{1,k}}$ are obtained from the 0th order residual tensor $\mathscr{W}_0$ as discussed in Section III. These subtensors are stored in a list and the subtensor which decreases the cost function the most is added to the tree structure under its parent node. Next, scale-2 subtensors belonging to the added node are created and added to the list. All of the scale-1 and scale-2 subtensors in the list are again evaluated to find the subtensor that minimizes the cost function. This procedure is repeated until the cost function $\mathbb{H}$ converges or the decrease is minimal. A pseudocode of the algorithm is given in Algorithm 2.

Algorithm 2 Multiscale HoSVD with Adaptive Pruning

1: Input: $\mathscr{X}$: tensor , $\mathbf{C} = (c_1, c_2, ..., c_N)$: the desired number of clusters for each modes, s_H: the highest scale of MS-HoSVD.
2: Output: T: Tree structure containing the MS-HoSVD decomposition of $\hat{\mathscr{X}}$.
3: Create an empty tree T.
4: Create an empty list L.
5: Add node containing $\mathscr{X}$ to L.
6: **while** There is a node in L that decreases the cost function $\mathbb{H}(T)$. **do**
7: Find the node corresponding to $\mathscr{X}_{s,t}$ (the tth subtensor from sth scale) in the list L that decreases $\mathbb{H}$ the most where $s \in \{0, ..., s_H\}$ and $t \in \{1, ..., K^s\}$.
8: $\mathscr{C}_{s,t}, \left\{\hat{\mathbf{U}}_{s,t}^{(n)}\right\} \leftarrow$ truncatedHOSVD($\mathscr{X}_{s,t}$).
9: Add the node containing $\mathscr{C}_{s,t}, \left\{\hat{\mathbf{U}}_{s,t}^{(n)}\right\}$ to T.
10: **if** $s < s_H$ **then**
11: Compute $\mathscr{W}_{s,t} = \mathscr{X}_{s,t} - \hat{\mathscr{X}_{s,t}}$.
12: Create K subtensors $\mathscr{X}_{s+1,K(t-1)+k}$ with $J_{s+1,K(t-1)+k}^{n}$ from $\mathscr{W}_{s,t}$ where $k \in \{1, 2, ..., K\}$ and $n \in \{1, 2, ..., N\}$.
13: Add K nodes containing $\mathscr{X}_{s+1,K(t-1)+k}$ and $\left\{J_{s+1,K(t-1)+k}^{n}\right\}$ to L.
14: **end if**
15: **end while**

VI. Data Reduction

In this section, we demonstrate the performance of MS-HoSVD for compressing different higher-order datasets, including functional connectivity brain networks, hyperspectral image and video, compared with HoSVD and Wavelet transform. We also compare MS-HoSVD to HoSVD for data reduction by using fixed rank selection and adaptive rank selection criteria for low-rank tensor approximations. Moreover, we show the performance of tree prunning strategy for data reduction.

A. Datasets

The proposed multiscale approach is applied to tensors including three different datasets and compared with HoSVD in terms of reconstruction error and compression rate. In the tables and figures below the error rate refers to the normalized tensor approximation error $\frac{\|\mathscr{X} - \hat{\mathscr{X}}\|_F}{\|\mathscr{X}\|_F}$ and the compression rate is computed as $\frac{\text{\# total bits to store } \hat{\mathscr{X}}}{\text{\# total bits to store } \mathscr{X}}$.

1) ERN dataset: The proposed approach is applied to a set of functional connectivity graphs constructed from EEG data containing the error-related negativity (ERN). The ERN is a brain potential response that occurs following performance errors in a speeded reaction time task usually 25-75 ms after the response [36]. Previous work [37] indicates that there is increased coordination between the lateral prefrontal cortex (lPFC) and medial prefrontal cortex (mPFC) within the theta frequency band (4-8 Hz) and ERN time window. EEG data

from 63-channels was collected in accordance with the 10/20 system on a Neuroscan Synamps2 system (Neuroscan, Inc.) sampled at 128 Hz from 91 subjects. Full methodological details of the recording are available in a previous paper [36]. The task was a common speeded-response letter (H/S) Flanker, where error and correct response-locked trials from each subject were utilized. A random subset of correct trials was selected, to equate the number of error relative to correct trials for each participant. The EEG data are pre-processed by the spherical spline current source density (CSD) waveforms to sharpen event-related potential (ERP) scalp topographies and reduce volume conduction [38]. For each subject and response type, the pairwise phase locking value in the theta frequency band was computed as described in [39].

A 4-mode tensor $\mathscr{X}_t \in \mathbb{R}^{63\times63\times91\times256}$ is created for ERN data where the first and second modes represent the adjacency matrix of the connectivity graphs while the third and fourth modes correspond to the subjects and time points, respectively.

2) PIE dataset: A 3-mode tensor $\mathscr{X} \in \mathbb{R}^{244\times320\times138}$ is created from PIE dataset [40]. The tensor contains 138 images from 6 different yaw angles and varying illumination conditions collected from a subject where each image is converted to gray scale. Fig. 1 illustrates the images from different frames of the PIE dataset.

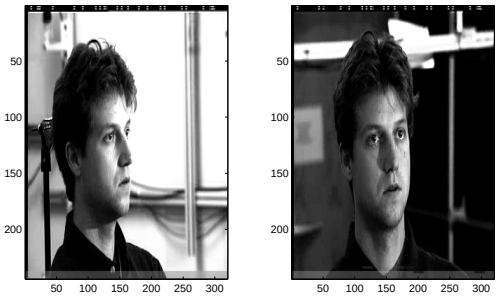

Fig. 1: Sample frames from PIE dataset corresponding to the 30th (left) and 80th (right) frames.

3) Hyperspectral Image: In this experiment, we used a hyperspectral image from [41] to create a 3-mode tensor $\mathscr{X} \in \mathbb{R}^{201\times250\times148}$ where the modes are rows, columns and spectral bands, respectively. Fig. 2 illustrates the images from different spectral bands of the hyperspectral image.

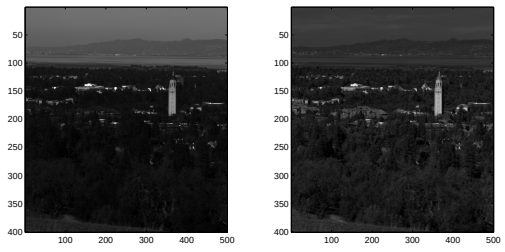

Fig. 2: Sample images from hyperspectral image corresponding to the 30th (left) and 80th (right) spectral band.

B. Data Reduction with Fixed Rank

In the following experiments, clustering is performed by LSA and the cluster number along each mode is chosen as $c_i = 2$. The rank used in HoSVD is selected based on the size of the datasets and gradually increased to illustrate the relationship between reconstruction error and compresion rate. In MS-HoSVD with 1-scale, rank of each scale is selected according to the criterion $R_1 \leq \frac{R_0}{c^{(N-1)}}$ derived in Section III-A. As seen in Fig. 3, MS-HoSVD provides better compression performance for all datasets. Moreover, selecting a smaller multilinear rank yielding lower compression rate increases the normalized reconstruction error for both MS-HoSVD and HoSVD as expected. Therefore, as the compression rate goes down the performance of HoSVD and MS-HoSVD become comparable to each other.

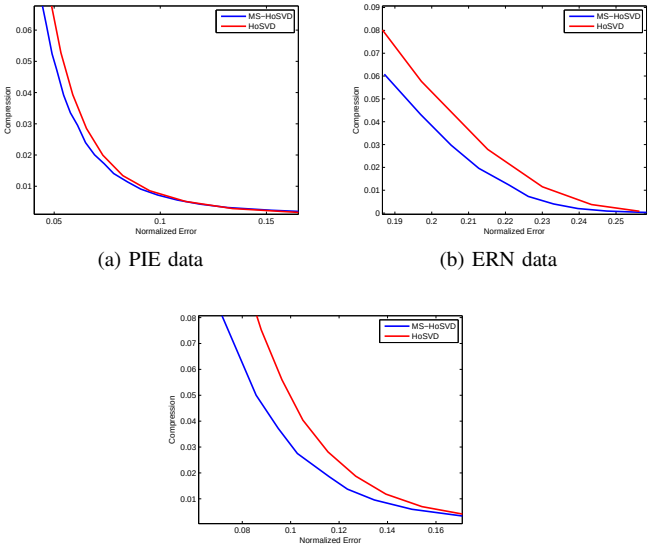

(a) PIE data (b) ERN data

(c) HSI

Fig. 3: Compression rate versus Normalized Error for MS-HoSVD (blue line) and HoSVD (red line) for a) PIE dataset, b) ERN data and c) HSI image with fixed rank criterion. MS-HoSVD provides better compression performance with lower compression rate for all datasets.

C. Data Reduction with Adaptively Chosen Rank

In this section, we evaluate the performance of MS-HoSVD for 1 and 2-scale decompositions compared to HoSVD and 3D and 4D Wavelet transform. In the following experiments, clustering is performed by LSA and the cluster number along each mode is chosen as $c_i = 2$. The rank used in HoSVD is selected adaptively using the energy criterion as described in Section III. In our experiments, we performed MS-HoSVD with $\tau = 0.7$ and $\tau = 0.75$ and we kept τ the same for each scale. For HoSVD, τ is gradually increased to illustrate the relationship between reconstruction error and compression rate.

Table VII explores the interplay between compression ratio and approximation error for MS-HoSVD in comparison to HoSVD and 4D-Wavelet for ERN dataset. For the 4-D Wavelet

compression, a 2-scale 1-D Wavelet transform followed by a 2-scale 3-D Wavelet transform with Daubechies 3 wavelet function were applied. Comparing MS-HoSVD with HoSVD, MS-HoSVD outperforms HoSVD with respect to varying error and compression rates. As expected, the addition of the second scale subtensors decreases the error rate while reducing the compression rate. In comparison to the wavelet transform, we observed that the particular order of applying the 1D and 3D wavelet transforms influences the performance. First, we applied 1D wavelet transform along the temporal mode followed by a 3D wavelet transform. In the second version of the implementation, we applied 1D wavelet transform along the subject mode followed by a 3D wavelet transform. As seen in Table VII, MS-HoSVD outperforms the Wavelet when 1D Wavelet transform is applied along the subject mode. However, when the 1D wavelet transform is applied along the temporal mode, the performance of 4D Wavelet transform becomes better than MS-HoSVD as the wavelet transform is powerful in capturing temporal correlation. Since the subjects are not ordered in terms of their similarity, the wavelet transform cannot compress along this dimension as efficiently as the temporal mode.

As seen in Tables VIII and IX, MS-HoSVD outperforms HoSVD with respect to compressing PIE and HSI data sets. Moreover, adding 2nd scale slightly improves the performance of MS-HoSVD. Fig. 4 illustrates the influence of scale on approximation quality. As expected, introducing additional finer scales into a multiscale approximation of video data improves image detail in each frame. However, 3D-Wavelet provides better performance than MS-HoSVD for PIE video but not for HSI. The 3rd mode of HSI corresponds to the wavelength and the correlation in this mode may not be as high as the correlation along the time dimension of a video sequence.

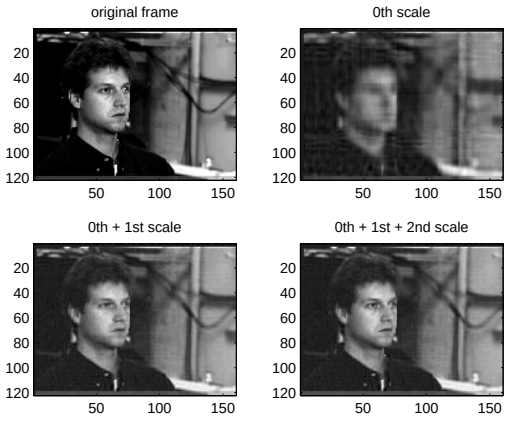

Fig. 4: A single frame of the PIE dataset showing increasing accuracy with scale.

D. Data Reduction with Adaptive Tree Prunning

In this section, we evaluate the performance of adaptive tree pruning multiscale decompositions. In the pruning experiments, clustering is performed by LSA and the cluster number along each mode is chosen as $c_i = 2$. The rank used in HoSVD is selected adaptively based on the energy threshold which is 0.7. A pruned version of MS-HoSVD with 2-scale analysis that minimizes the cost function $\mathbb{H} = Error + \eta \cdot Compression$ is implemented for PIE, ERN, and HSI datasets with varying η values as reported in Tables X, XI, and XII. As η increases, reducing the compression rate becomes more important and the algorithm prunes the leaf nodes more. For example, a choice of $\eta \geq 0.75$ prunes all of the nodes corresponding to the second scale subtensors (Tables X, XI, and XII).

Fig. 5 illustrates the performance of the pruning algorithm on PIE dataset. Applying pruning with $\eta = 0.25$ increases the reconstruction error from 0.0276 to 0.0506 while providing four times increased compression performance (Table XII). As seen in Fig. 5, the 2nd scale approximation obtained by adaptive pruning algorithm preserves most of the facial details in the image.

TABLE VII: Normalized reconstruction error computed for compression of a 4-mode ERN tensor using MS-HoSVD, HoSVD and 4D-Wavelet transform. Two versions of 4D wavelet transform are implemented as 1D wavelet transform along the temporal mode followed by a 3D wavelet transform (4D-Wavelet-T) and 1D wavelet transform along the subject mode followed by a 3D wavelet transform (4D-Wavelet-S).

ERN	data size: $63 \times 63 \times 91 \times 256$		
	τ	Compression	Error
MS-HoSVD (1 scale)	0.70	0.1912	0.1609
MS-HoSVD (1 scale)	0.75	0.2996	0.1425
MS-HoSVD (2 scale)	0.70	0.3827	0.1266
MS-HoSVD (2 scale)	0.75	0.5585	0.1036
HoSVD		0.1967	0.1835
HoSVD		0.2920	0.1654
HoSVD		0.3828	0.1490
HoSVD		0.5455	0.1212
4D-Wavelet-T		0.1889	0.1228
4D-Wavelet-T		0.3066	0.0937
4D-Wavelet-S		0.1907	0.2076
4D-Wavelet-S		0.2985	0.1936
4D-Wavelet-S		0.3806	0.1867
4D-Wavelet-S		0.5435	0.1784

TABLE VIII: Normalized reconstruction error computed for compression of a video from PIE data using MS-HoSVD, HoSVD and 3D-Wavelet transform.

PIE	data size: $244 \times 320 \times 138$		
	τ	Compression	Error
MS-HoSVD (1 scale)	0.70	0.0261	0.0540
MS-HoSVD (1 scale)	0.75	0.0563	0.0410
MS-HoSVD (2 scale)	0.70	0.1241	0.0276
MS-HoSVD (2 scale)	0.75	0.2330	0.0206
HoSVD		0.0261	0.0566
HoSVD		0.0575	0.0434
HoSVD		0.1274	0.0317
HoSVD		0.2388	0.0230
3D-Wavelet		0.0262	0.0617
3D-Wavelet		0.0579	0.0360
3D-Wavelet		0.1286	0.0171
3D-Wavelet		0.2300	0.0083

VII. Classification

In this section, we evaluate the features extracted from MS-HoSVD for classification of 2-mode and 3-mode tensors con-

TABLE IX: Normalized reconstruction error computed for compression of a hyperspectral image using MS-HoSVD, HoSVD and 3D-Wavelet transform.

HSI	data size: $201 \times 250 \times 148$		
	τ	Compression	Error
MS-HoSVD (1 scale)	0.70	0.0301	0.0570
MS-HoSVD (1 scale)	0.75	0.0522	0.0457
MS-HoSVD (2 scale)	0.70	0.1229	0.0258
MS-HoSVD (2 scale)	0.75	0.2100	0.0192
HoSVD		0.0303	0.0544
HoSVD		0.0529	0.0485
HoSVD		0.1259	0.0364
HoSVD		0.2110	0.0283
3D-Wavelet		0.0304	0.1002
3D-Wavelet		0.0525	0.0793
3D-Wavelet		0.1223	0.0442
3D-Wavelet		0.2135	0.0244

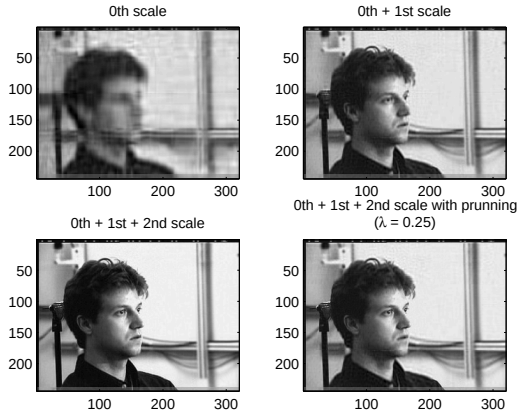

Fig. 5: Reconstruction error and compression rate computed for pruned tree structure obtained by applying MS-HoSVD with 2-scales to PIE dataset. Top-left and right image is the sample frame by reconstructing the tensor using only 0th scale and recontruction by using 0th and 1st scales respectively. Bottom-left image is a sample frame for reconstructed using 2-scale approximation with all the subtensors and the bottom-right image is the reconstruction of 2 scale analysis with pruning approach where $\eta = 0.25$.

taining object images and hand gesture videos. Discrimination performance of the MS-HoSVD features is also compared with the features extracted by HoSVD.

A. COIL-100 Image Dataset

The COIL-100 database contains 7200 images collected from 100 objects where the images of each object were taken at pose intervals of 5°. In Fig. 6, sample images collected from four object taken from different angles can be seen. Each image was downsampled to a gray-scale image of 32×32 pixels for computational efficiency. Number of images per object used for training data was gradually increased from 18 to 54 and selected randomly. A 3-mode tensor $\mathscr{X}_{tr} \in \mathbb{R}^{32 \times 32 \times I_{tr}}$ is constructed from training images where $I_{tr} \in 100 \times \{18,\ 36,\ 54\}$ and the rest of the images are used in the testing phase.

TABLE X: Reconstruction error and compression rate computed for pruned tree structure obtained by applying MS-HoSVD with 2-scales to hyperspectral image.

η	0	0.25	0.50	0.75	1
Normalized error	0.0258	0.0316	0.0528	0.0570	0.0570
Compression	0.1229	0.0849	0.0371	0.0301	0.0301
Scales of subtensors	0+1+2	0+1+2	0+1+2	0+1	0+1

TABLE XI: Reconstruction error and compression rate computed for pruned tree structure obtained by applying MS-HoSVD with 2-scales to ERN data.

η	0	0.25	0.50	0.75	1
Normalized error	0.1609	0.1657	0.1969	0.2155	0.2155
Compression	0.1912	0.1690	0.0826	0.0555	0.0555
Scales of subtensors	0+1+2	0+1+2	0+1	0+1	0+1

B. The Cambridge Hand Gesture Dataset

The Cambridge hand gesture database consists of 900 image sequences of nine gesture classes of three primitive hand shapes and three primitive motions where each class contains 100 image sequences (5 different illuminations $\times$ 10 arbitrary motions $\times$ 2 subjects). In Fig. 7, sample image sequences collected for nine hand gestures can be seen. Number of tensors used for training data gradually increased from 25 to 75 per gesture and selected randomly. 4-mode tensors $\mathscr{X}_{tr} \in \mathbb{R}^{30 \times 40 \times 30 \times I_{tr}}$ is constructed from training image sequences where $I_{tr} \in 9 \times \{25,\ 50,\ 75\}$ the rest of the image sequences are used in the testing phase.

C. Classification Experiments

1) Training: For HoSVD, the training tensor is decomposed as follows:

$$\mathscr{X}_{tr} = \mathscr{S}_{tr} \times_{n=1}^{N} \mathbf{U}_{tr}^{(n)}, \tag{30}$$

TABLE XII: Reconstruction error and compression rate computed for pruned tree structure obtained by applying MS-HoSVD with 2-scales to PIE data.

η	0	0.25	0.50	0.75	1
Normalized error	0.0276	0.0506	0.0538	0.0540	0.0540
Compression	0.1241	0.0377	0.0264	0.0261	0.0261
Scales of subtensors	0+1+2	0+1+2	0+1+2	0+1	0+1

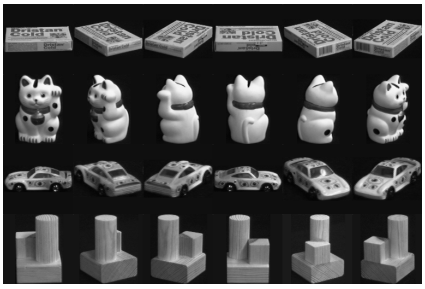

Fig. 6: Image samples of four different objects from COIL-100 dataset from varying pose angles (from 0° to 240° with 60° increments).

Fig. 7: Illustration of nine different classes in Cambridge Hand Gesture Dataset.

where $\mathscr{S}_{tr}$ is the core tensor and $\mathbf{U}_{tr}^{(n)}$s are the mode matrices. Mode matrices corresponding to the first $N-1$ modes are used to create feature vectors for each image as follows.

Let $\mathscr{X}_i$ be the ith sample from the training set. First, $\mathscr{X}_i$ is projected onto the subspaces $\mathbf{U}_{tr}^{(n)}$ for $n \in \{1,...,N-1\}$ to obtain the core tensor $\mathscr{S}_i = \mathscr{X}_i \times_{n=1}^{N-1} (\mathbf{U}^{(n)})^\top$ where $\mathscr{S}_i \in \mathbb{R}^{32\times32}$ and $\mathscr{S}_i \in \mathbb{R}^{30\times40\times30}$ for object images and hand gesture image sequences, respectively. Let $\mathbf{s}_i$ be the vector formed by vectorizing $\mathscr{S}_i$. Fisher score (FS) [42] is computed for all of the entries in $\mathbf{s}_i$ to form the feature vector $\mathbf{x}_i$ corresponding to each training sample $\mathscr{X}_i$. Nf number of features with the highest Fisher Score are selected to form a feature vector $\mathbf{x}_i \in \mathbb{R}^{Nf\times1}$ where the number of features (Nf) is determined by maximizing the classification score for both HoSVD and MS-HoSVD.

For MS-HoSVD, the training tensor $\mathscr{X}_{tr}$ is decomposed using 1-scale MS-HoSVD as follows. Clustering is performed by LSA and the cluster number along each mode is chosen as $c = \{2,\ 3,\ 1\}$ yielding 6 subtensors for COIL-100 dataset and $c = \{2,\ 2,\ 3,\ 1\}$ yielding 16 subtensors for hand gesture dataset. We did not cluster the last mode that corresponds to the classes to make the comparison with HoSVD fair. The rank used in 0th scale is selected adaptively depending on the energy criterion with $\tau = 0.7$, while full rank decomposition is used for the 1st scale. Unlike HoSVD, MS-HoSVD provides multiple mode matrices corresponding to 0th and 1st scales and all of these mode matrices correspond to the first $N-1$ modes are used to form the feature vector similar to the feature vectors obtained from HoSVD.

2) Testing: Feature vectors for the testing images are formed similar to the training features. First, all of the testing samples are projected onto $\mathbf{U}_{tr}^{(n)}$ where $n \in \{1,...,N-1\}$, then features corresponding to the training features are selected to form the feature vectors. Once the feature vectors are obtained, 1-NN is used to classify the test samples using the Euclidean distance.

As seen in Tables XIII and XIV, features obtained from MS-HoSVD have greater Fisher score on average and classify the images better than HoSVD. It is also seen that the performance of HoSVD and MS-HoSVD become close to each other as the size of the training dataset increases. The reason behind the improved performance of MS-HoSVD is that MS-HoSVD captures the variations and nonlinearities along the modes such as rotation or translation better than HoSVD, and both of the datasets used in this section have such a characteristic. Since these nonlinearities are encoded in the higher scale (1st scale) features while the average characteristics are captured by the lower scale (0th scale) MS-HoSVD features which are the same as the HoSVD, the classification performance of the MS-HoSVD is slightly better than HoSVD. However, MS-HoSVD features have much higher Fisher score than HoSVD features on average which indicates that classification using 1-NN with Euclidean distance may not be able to capture this difference in discrimination power since it treats all of the features obtained from 0th and 1st scales equally. Assigning different weights to MS-HoSVD features or using these features in a kernel approach such as kernel-SVM would provide bigger difference compared to HoSVD features.

TABLE XIII: 1NN classification results for COIL-100 dataset over 20 trials with $Nf = 100$.

I_{tr}	Method	Accuracy mean ± std.	FS (10^3) mean ± std.
1800	HoSVD	93.07 ± 1.33	0.2471 ± 0.0303
	MS-HoSVD	93.71 ± 1.28	1.1138 ± 0.3796
3600	HoSVD	97.10 ± 0.83	0.2445 ± 0.0173
	MS-HoSVD	97.41 ± 0.69	1.0141 ± 0.3839
5400	HoSVD	98.16 ± 0.72	0.2572 ± 0.0139
	MS-HoSVD	98.38 ± 0.65	0.9721 ± 0.3454

TABLE XIV: 1NN classification results for hand gesture dataset over 20 trials with $Nf = 200$.

I_{tr}	Method	Accuracy mean ± std.	FS (10^3) mean ± std.
25	HoSVD	75.01 ± 3.99	5.5102 ± 0.5044
	MS-HoSVD	75.40 ± 3.87	6.3709 ± 1.3514
50	HoSVD	83.15 ± 2.90	4.0065 ± 0.2100
	MS-HoSVD	83.86 ± 3.12	6.0433 ± 1.6775
75	HoSVD	86.93 ± 2.31	3.6750 ± 0.1663
	MS-HoSVD	87.47 ± 2.07	5.1396 ± 1.5677

VIII. Conclusions

In this paper, we proposed a new multi-scale tensor decomposition technique for better approximating the local nonlinearities in generic tensor data. The proposed approach constructs a tree structure by considering similarities along different fibers of the tensor and decomposes the tensor into lower dimensional subtensors hierarchically. A low-rank approximation of each subtensor is then obtained by HoSVD. We also introduced a pruning strategy to find the optimum tree structure by keeping the important nodes and eliminating redundancy in the data. The proposed approach is applied to a set of 3-way and 4-way tensors containing simulated and real datasets to evaluate its performance on both data reduction and classification applications.

It is important to note that even though there are other established methods for higher order data reduction such as 3D and 4D wavelets, the proposed method does not rely on the structure of the data. For example, wavelet based methods work well when one of the modes is time as they take advantage of temporal correlation. The proposed method, on the other hand, is universal as it can be applied to higher order data obtained across different variates.

Future work will consider automatic selection of parameters such as the number of clusters and the appropriate rank along each mode. Adapting the method to dynamic tensors for identifying structural changes to the tensor in time will also be considered. Parallelization of the algorithm such as parallel construction of subtensors and parallel implementation of HoSVD will be considered for an efficient implementation of the algorithm [43]. Faster implementation will also enable us to implement finer scale decompositions. Proposed algorithm currently constructs the tree structure based on decomposing the tensor using HoSVD. The proposed tensor decomposition structure can also be implemented using other tensor decomposition methods such as PARAFAC and tensor-train decompositions.

REFERENCES

[1] D.Letexier *et al.*, "Nonorthogonal tensor matricization for hyperspectral image filtering," *Geoscience and Remote Sensing Letters, IEEE*, vol. 5, no. 1, pp. 3–7, 2008.

[2] T.-K.Kim and R.Cipolla, "Canonical correlation analysis of video volume tensors for action categorization and detection," *Pattern Analysis and Machine Intelligence, IEEE Transactions on*, vol. 31, no. 8, pp. 1415–1428, 2009.

[3] F.Miwakeichi *et al.*, "Decomposing eeg data into space–time–frequency components using parallel factor analysis," *NeuroImage*, vol. 22, no. 3, pp. 1035–1045, 2004.

[4] A.Cichocki *et al.*, "Tensor decompositions for signal processing applications: From two-way to multiway component analysis," *IEEE Signal Processing Magazine*, vol. 32, no. 2, pp. 145–163, 2015.

[5] I. V.Oseledets, "Tensor-train decomposition," *SIAM Journal on Scientific Computing*, vol. 33, no. 5, pp. 2295–2317, 2011.

[6] L.De Lathauwer, "Decompositions of a higher-order tensor in block terms-part ii: definitions and uniqueness," *SIAM Journal on Matrix Analysis and Applications*, vol. 30, no. 3, pp. 1033–1066, 2008.

[7] L.Cheng *et al.*, "Probabilistic tensor canonical polyadic decomposition with orthogonal factors," *IEEE Transactions on Signal Processing*, vol. 65, no. 3, pp. 663–676, 2015.

[8] X.Fu *et al.*, "Joint tensor factorization and outlying slab suppression with applications," *IEEE Transactions on Signal Processing*, vol. 63, no. 23, pp. 6315–6328, 2015.

[9] T. G.Kolda and B. W.Bader, "Tensor decompositions and applications," *SIAM review*, vol. 51, no. 3, pp. 455–500, 2009.

[10] L.De Lathauwer *et al.*, "A multilinear singular value decomposition," *SIAM journal on Matrix Analysis and Applications*, vol. 21, no. 4, pp. 1253–1278, 2000.

[11] T.Jiang and N. D.Sidiropoulos, "Kruskal's permutation lemma and the identification of candecomp/parafac and bilinear models with constant modulus constraints," *IEEE Transactions on Signal Processing*, vol. 52, no. 9, pp. 2625–2636, 2004.

[12] A.Shashua and T.Hazan, "Non-negative tensor factorization with applications to statistics and computer vision," in *Proceedings of the 22nd international conference on Machine learning*. ACM, 2005, pp. 792–799.

[13] A.Cichocki *et al.*, "Non-negative tensor factorization using alpha and beta divergences," in *Acoustics, Speech and Signal Processing, 2007. ICASSP 2007. IEEE International Conference on*, vol. 3. IEEE, 2007, pp. III–1393.

[14] A.Cichocki *et al.*, "Novel multi-layer non-negative tensor factorization with sparsity constraints," in *International Conference on Adaptive and Natural Computing Algorithms*. Springer, 2007, pp. 271–280.

[15] M. E.Kilmer *et al.*, "Third-order tensors as operators on matrices: A theoretical and computational framework with applications in imaging," *SIAM Journal on Matrix Analysis and Applications*, vol. 34, no. 1, pp. 148–172, 2013.

[16] Z.Zhang and S.Aeron, "Exact tensor completion using t-svd," *IEEE Transactions on Signal Processing*, 2016.

[17] L.Grasedyck, "Hierarchical singular value decomposition of tensors," *SIAM Journal on Matrix Analysis and Applications*, vol. 31, no. 4, pp. 2029–2054, 2010.

[18] S. K.Suter *et al.*, "Tamresh–tensor approximation multiresolution hierarchy for interactive volume visualization," in *Computer Graphics Forum*, vol. 32, no. 3pt2. Wiley Online Library, 2013, pp. 151–160.

[19] M. A. O.Vasilescu and D.Terzopoulos, "Multilinear image analysis for facial recognition," in *Pattern Recognition, 2002. Proceedings. 16th International Conference on*, vol. 2. IEEE, 2002, pp. 511–514.

[20] J.Yang *et al.*, "Two-dimensional pca: a new approach to appearance-based face representation and recognition," *Pattern Analysis and Machine Intelligence, IEEE Transactions on*, vol. 26, no. 1, pp. 131–137, 2004.

[21] X.He *et al.*, "Tensor subspace analysis," in *Advances in neural information processing systems*, 2005, pp. 499–506.

[22] X.Niyogi, "Locality preserving projections," in *Neural information processing systems*, vol. 16. MIT, 2004, p. 153.

[23] G.Dai and D.-Y.Yeung, "Tensor embedding methods," in *Proceedings of the National Conference on Artificial Intelligence*, vol. 21, no. 1. Menlo Park, CA; Cambridge, MA; London; AAAI Press; MIT Press; 1999, 2006, p. 330.

[24] H.-T.Chen *et al.*, "Local discriminant embedding and its variants," in *Computer Vision and Pattern Recognition, 2005. CVPR 2005. IEEE Computer Society Conference on*, vol. 2. IEEE, 2005, pp. 846–853.

[25] X.He *et al.*, "Neighborhood preserving embedding," in *Computer Vision, 2005. ICCV 2005. Tenth IEEE International Conference on*, vol. 2. IEEE, 2005, pp. 1208–1213.

[26] X.Li *et al.*, "Discriminant locally linear embedding with high-order tensor data," *Systems, Man, and Cybernetics, Part B: Cybernetics, IEEE Transactions on*, vol. 38, no. 2, pp. 342–352, 2008.

[27] V.De Silva and L.-H.Lim, "Tensor rank and the ill-posedness of the best low-rank approximation problem," *SIAM Journal on Matrix Analysis and Applications*, vol. 30, no. 3, pp. 1084–1127, 2008.

[28] A.Özdemir *et al.*, "Multiscale tensor decomposition," in *Signals, Systems and Computers, 2016 50th Asilomar Conference on*. IEEE, 2016, pp. 625–629.

[29] A.Ozdemir *et al.*, "Locally linear low-rank tensor approximation," in *Signal and Information Processing (GlobalSIP), 2015 IEEE Global Conference on*. IEEE, 2015, pp. 839–843.

[30] J.Yan and M.Pollefeys, "A general framework for motion segmentation: Independent, articulated, rigid, non-rigid, degenerate and non-degenerate," in *Computer Vision–ECCV 2006*. Springer, 2006, pp. 94–106.

[31] A.Karami *et al.*, "Compression of hyperspectral images using discerete wavelet transform and tucker decomposition," *IEEE journal of selected topics in applied earth observations and remote sensing*, vol. 5, no. 2, pp. 444–450, 2012.

[32] M.Iwen and B.Ong, "A distributed and incremental svd algorithm for agglomerative data analysis on large networks," *SIAM Journal on Matrix Analysis and Applications*, vol. 37, no. 4, pp. 1699–1718, 2016.

[33] N.Vannieuwenhoven *et al.*, "A new truncation strategy for the higher-order singular value decomposition," *SIAM Journal on Scientific Computing*, vol. 34, no. 2, pp. A1027–A1052, 2012.

[34] K.Ramchandran and M.Vetterli, "Best wavelet packet bases in a rate-distortion sense," *IEEE Transactions on Image Processing*, vol. 2, no. 2, pp. 160–175, 1993.

[35] P.Pudil *et al.*, "Floating search methods in feature selection," *Pattern recognition letters*, vol. 15, no. 11, pp. 1119–1125, 1994.

[36] J. R.Hall *et al.*, "Externalizing psychopathology and the error-related negativity," *Psychological Science*, vol. 18, no. 4, pp. 326–333, 2007.

[37] J. F.Cavanagh *et al.*, "Prelude to and resolution of an error: Eeg phase synchrony reveals cognitive control dynamics during action monitoring," *The Journal of Neuroscience*, vol. 29, no. 1, pp. 98–105, 2009.

[38] J.Kayser and C. E.Tenke, "Principal components analysis of laplacian waveforms as a generic method for identifying erp generator patterns: Ii. adequacy of low-density estimates," *Clinical neurophysiology*, vol. 117, no. 2, pp. 369–380, 2006.

[39] S.Aviyente *et al.*, "A phase synchrony measure for quantifying dynamic functional integration in the brain," *Human brain mapping*, vol. 32, no. 1, pp. 80–93, 2011.

[40] T.Sim *et al.*, "The cmu pose, illumination, and expression database," *Pattern Analysis and Machine Intelligence, IEEE Transactions on*, vol. 25, no. 12, pp. 1615–1618, 2003.

[41] T.Skauli and J.Farrell, "A collection of hyperspectral images for imaging systems research," in *IS&T/SPIE Electronic Imaging*. International Society for Optics and Photonics, 2013, pp. 86 600C–86 600C.

[42] Q.Gu *et al.*, "Generalized fisher score for feature selection," *arXiv preprint arXiv:1202.3725*, 2012.

[43] A. P.Liavas and N. D.Sidiropoulos, "Parallel algorithms for constrained tensor factorization via alternating direction method of multipliers," *IEEE Transactions on Signal Processing*, vol. 63, no. 20, pp. 5450–5463, 2015.